Airborne Gravity Data Reconstruction Strategies for Geoid Optimization in Peninsular Malaysia

Zamri, A. N. M.,[1] Pa'suya, M. F.,[1*] Din, A. H. Md.,[2] Abbak, R. A.,[3] Ali, T. A. T.,[1] Talib, N.,[1] Azmin, N. S. H. N.[1] and Othman, N. A.[1]

[1]Environment and Climate Change Research Group (ECC), College of Built Environment, Universiti Teknologi MARA, Perlis Branch, Arau Campus, 02600 Arau, Perlis, Malaysia
E-mail: afreenanisha99@gmail.com, faiz524@uitm.edu.my,* tengkuafrizal@uitm.edu.my, noorf492@uitm.edu.my, nurushafiqahazelin@gmail.com, hurulain9818@gmail.com

[2]Geospatial Imaging and Information Research Group (GI2RG), Faculty of Built Environment and Surveying, Universiti Teknologi Malaysia, 81310 Johor Bahru, Johor, Malaysia, E-mail: amihassan@utm.my

[3]Department of Geomatics Engineering, Konya Technical University, Konya, Turkiye
E-mail: raabbak@ktun.edu.tr

**Corresponding Author*

DOI: https://doi.org/10.52939/ijg.v21i6.4239

Abstract

Geoid height is essential for precise height determination, particularly in surveying and geodetic applications. Airborne gravity data substantially improve geoid models, especially over regions with complex terrain where terrestrial coverage is limited. However, since airborne data are acquired at flight altitude, they require downward continuation to the geoid surface which an inherently unstable process. Despite ongoing advancements, the most effective strategy for combining and gridding gravity data, particularly airborne measurements, remains a topic of research. This study evaluates two downward continuation strategies to assess their influence on geoid accuracy. The first strategy applies downward continuation to airborne data simultaneously with terrestrial and marine data, incorporating a range of buffer distances (0 km, 1 km, 5 km, and 10 km) to examine their effect on model performance. The second strategy involves performing downward continuation on airborne data independently before merging with other datasets. Numerical results indicate the Root Mean Square Error (RMSE) values of 0.044 m for the first strategy and 0.045 m for the second, with a marginal difference of 0.001 m. Although the difference appears minor, even marginal improvements can be pivotal in high-precision geoid modelling particularly in localized regions where complex topography or sparse data coverage may magnify subtle errors. Such refinements are essential to advancing the long-term goal of achieving geoid accuracy at the 1 cm level for Peninsular Malaysia.

Keywords: Airborne, Downward Continuation, Gravimetric Geoid, KTH Method, Peninsular Malaysia

1. Introduction

Geoid is a crucial element particularly in surveying field concerning the derivation of height coinciding with mean sea level (MSL). It is relatively representing the equipotential surface of earth's gravity field [1]. Achieving exceptional precision in determining geoid height stands as a pivotal pursuit for geodesists, who played a crucial role in this endeavor. Precision in geoid height determination holds paramount importance, particularly in deriving precise orthometric heights on the Earth's surface through Global Navigation Satellite System (GNSS) observations. In the Malaysian geodetic research community, determining precise geoid models has become a top priority, aiming for an accuracy of 1 cm in flat and moderate topography regions and 10 cm in high elevation areas, as emphasized by [2] and [3]. The key obstacle in producing an accurate geoid model is the lack of understanding regarding the impact of quantitative factors, including the input dataset used in geoid modelling software [4]. Disclosing the exact main factor is challenging because various factors may slightly affect the accuracy of the geoid. While the theoretical disparities are well understood, exploring practical applications becomes imperative to attain optimal results.

Airborne gravity data has been identified in [5] and [6] as instrumental in enhancing geoid model, especially in areas with limited accessibility or challenging topography. In the last two decades, a number of nations have acknowledged that airborne gravity data can alleviate the time-consuming and labor-intensive nature of terrestrial gravity data collection, numerous countries have initiated airborne gravity campaigns to enhance the refinement of geoid models within their territories (e.g., Malaysia, Indonesia, the USA, Turkey, New Zealand, Australia, the Philippines, and Thailand). Back in 2002, Malaysia has utilized airborne gravity data to address the deficiency in gravity data coverage across the Malaysian region especially over hardly accessible areas [7]. Prior conducting geoid modeling, standard procedures in most available methods for geoid computation require data input in grid format. Although the significance of airborne gravity data in enhancing geoid accuracy is well established, considerable challenges remain in the optimal integration and gridding of these datasets. This extends beyond the well-known instability of downward continuation as the airborne gravity needs to downward continuation to the topography surface before combining with others gravity data [8][9] and [10]. Literature records found that a numbers of studied have been discussed the downward continuation methods (e.g., [11][12] and [13] but the 3D Least Square Collocation (3D-LSC) indeed stands out as a novel method for combining and gridding gravity data. Its versatility lies in its ability to simultaneously perform downward continuation of airborne data while integrating it with other gravity data sources, streamlining the process into a single procedure [14].

However, the challenge arises to involve integrating the various sources of gravity data with differing levels of accuracy as choosing grid resolution introduces a critical trade-off the inconsistencies in data acquisition parameters such as varying flight altitudes, track spacing, and data density further complicate gridding and require adaptive filtering and weighting strategies [8]. In fact, the accuracy of terrestrial gravity data is more precise than airborne gravity data and without proper procedure in the combine and gridding process, the accuracy of terrestrial gravity data will be influenced by the airborne gravity. This process is inherently ill-posed, where even minimal noise in airborne gravity data can be severely amplified when projected to the geoid surface particularly for high-altitude surveys as stated in [15] and [16]. This underscores that the problem is not merely one of downward continuation, but also of determining the most effective resolution, filtering, and interpolation strategies to integrate multi-source gravity data. The absence of standardized evaluation frameworks for these techniques further complicates the development of robust geoid models, particularly in complex coastal regions like Peninsular Malaysia. Consequently, this study addresses these unresolved aspects by evaluating and optimizing the full workflow of data integration and gridding in support of accurate regional geoid determination.

This study explored the optional strategy for effectively combining and gridding airborne gravity data based on two different strategies. The first strategy is the common method using 3D-LSC, which combine all input data in a single procedure [17]. The airborne gravity data are simultaneously downward from flight height to topographical surface while combining and gridding it concurrently. The main superiority of this method is its capability to accommodate heterogeneous data of different types and spatial resolutions. However, its application to massive datasets over large areas is hindered by excessive computational efforts [18]. Given the dominance of airborne data compared to terrestrial data used in this study, an in-depth analysis of buffer distances was conducted to assess their impact on gravimetric geoid accuracy. The second strategy involves two-step processing approach, where the process of downward continuation of airborne gravity data is executed separately before combined and grided with other data. Subsequently, this combined dataset is gridded and utilized to compute the gravimetric geoid using the KTH method. The results of both strategies have been verified with GNSS levelling data obtained from Department of Survey and Mapping Malaysia (DSMM). A comparative analysis of these two strategies has been performed to determine the optimal method in combining and gridding gravity data, serving the primary objective of this study.

2. Study Area and Datasets

2.1 Study Area

Geoid models in this study covers the Peninsular Malaysia area as shown in Figure 1. The final gravimetric geoids are interpolated over a spatial extent of 7°45′ × 7°45′, encompassing the latitude spanning from 0°00′N to 7°45′N and longitude spanning 98°00′E to 105°45′E.

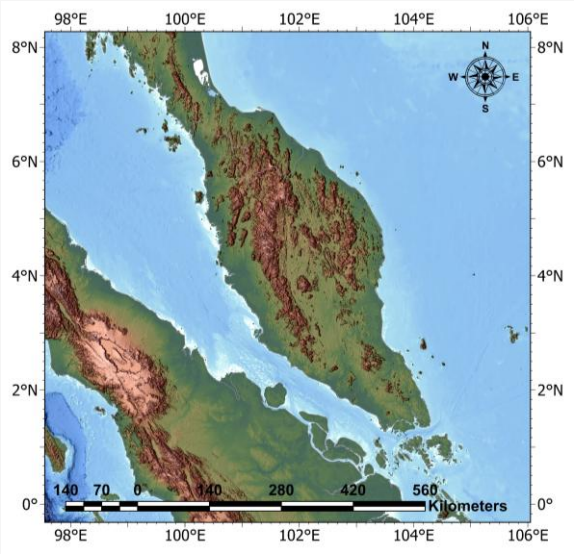

Figure 1: Study Area (Peninsular Malaysia)

2.2 Dataset Used

2.2.1 Terrestrial gravity

The collection of the terrestrial gravity data in Malaysia was commenced in 1988 through the collaborative efforts of the DSMM [19]. It is well-known that terrestrial gravity is predominantly feasible in flat and moderate areas, while airborne gravity data are acquired to cover the high mountainous regions. However, the utilization of multiple data acquisition methods inevitably introduced redundancies and duplicate points within the dataset. To mitigate this issue and ensure the integrity of subsequent geoid computations, a rigorous process of data filtering and elimination was undertaken through cross-validation techniques. Through rigorous filtering processes, redundant data points were systematically identified and removed, thereby refining the dataset for enhanced accuracy can be available. In total, a substantial dataset comprising 7,944 terrestrial gravity data points in Figure 2(a) was employed in the computation of the geoid model.

2.2.2 Airborne Gravity

Airborne gravity data is crucial as an additional dataset required to cover inaccessible areas, particularly at high elevations where ground gravimeter surveys are impractical. The utilization of airborne gravity data in Malaysia can be traced back to 2002 when DSMM collaborated with the Danish agency Kort & Matrikelstyrensen (KMS) to conduct comprehensive surveys. This collaborative effort involved the utilization of two distinct aircraft models to collect airborne gravity data: the Antonov-38 aircraft for capturing data over land areas and the Beechcraft-BE200 for surveying marine regions, ensuring a comprehensive coverage across diverse terrain types with flying altitude of less than 4500 m [20]. In this present study, a substantial dataset comprising a total of 24,855 airborne gravity data points has been incorporated. The distribution of these data points across the study area in Figure 2(b) provides insights into the spatial distribution and coverage of the airborne gravity data within Peninsular Malaysia.

2.2.3 Satellite-Derived marine gravity

Gravity anomalies data for marine regions were collected from the Sandwell model which is based upon the satellite altimeter data. This comprehensive dataset is publicly accessible via the official website at https://topex.ucsd.edu/cgi-bin/get_data.cgi [21]. However, it is unpractical to directly utilized the data in the computation as gravity anomalies at coastal area are particularly problematic [22]. To mitigate potential inaccuracies, a pragmatic approach was adopted where data specifically within a 20-kilometer radius from the coastal areas were removed from the dataset. Satellite altimeters work well over the open ocean where radar signals reflect cleanly off the sea surface. However, proximity to land introduces signal distortion due to the interference of simultaneous reflections from both land and water, making them less reliable [23]. Standard processing systems are optimized for ocean-only signals and often reject these mixed coastal returns, especially within 10 - 20 kilometres from the shore [24]. As a result, the number of satellite-derived marine gravity data points utilized in this study was refined to 175,193 points as depicted in Figure 2(c).

2.2.4 Global Geopotential Model (GGM)

Gravity Global Geopotential Model (GGM) is necessary in geoid computation to accurately interpolate the geoid height that closely represent the undulation of earth gravitational model locally and globally. This research employs the most recent combined-type GGM model, specifically XGM2019 as depicted Figure 2(d) and Table 1. The data were captured using combination of Altimetry, Satellite (GOCO06s), ground data and topography which capable to capture more detail and precise representation of GGM model. It was published in 2019 which readily available via the official website (https://icgem.gfz-potsdam.de/homeA) [25].

2.2.5 Global Digital Elevation Model (GDEM)

Global Digital Elevation Model (GDEM) data serves as essential input to mitigate the terrain effects in gravity data reconstruction.

Table 1: Properties of GGM input

Model	Year	Degree	Input Data	Reference
XGM2019	2019	360	A - Altimetry, G - Ground Data, S - Satellite (GOCO06s), T - Topography	[25]

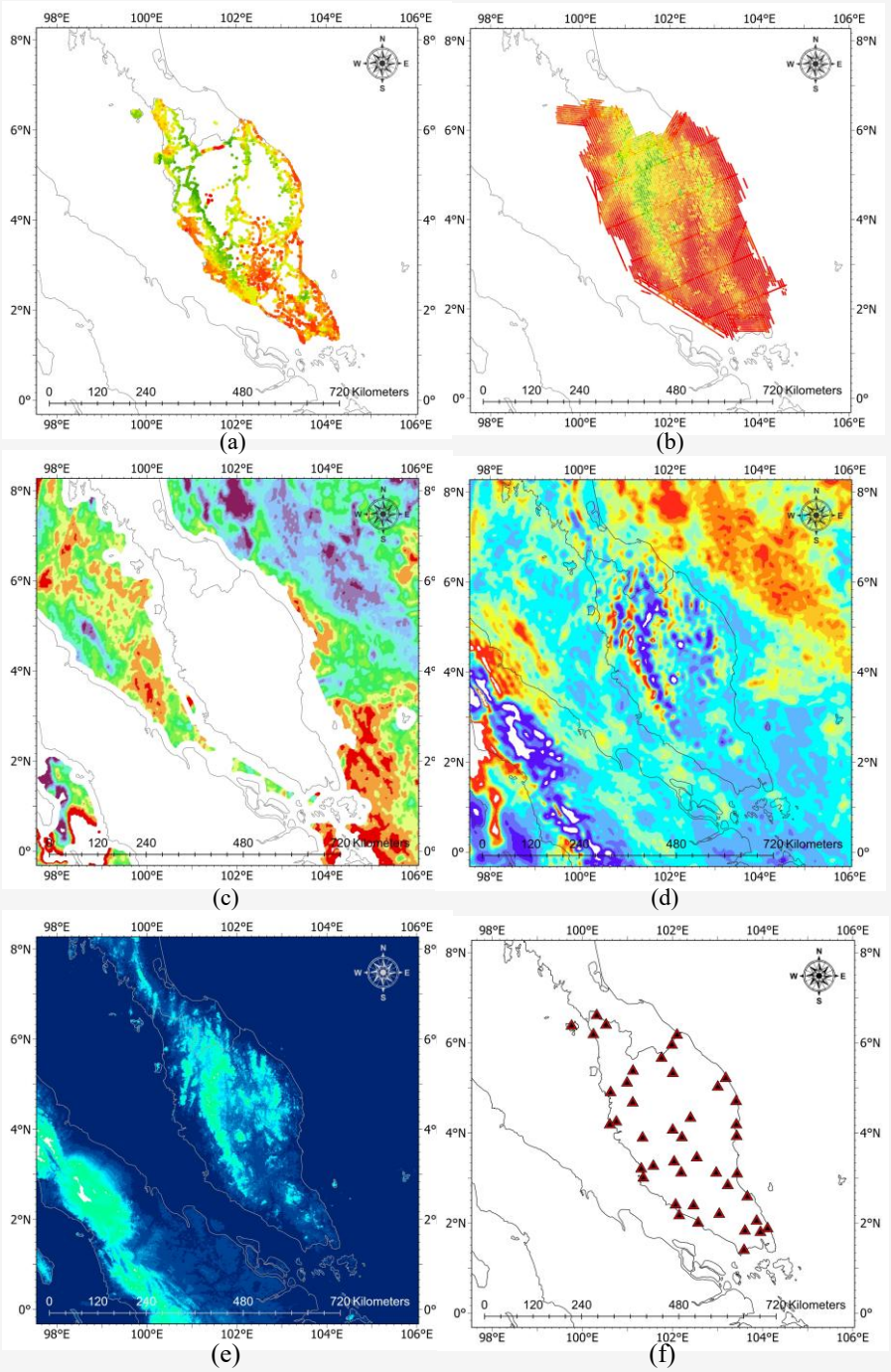

Figure 2: Dataset utilized in this study encompassed (a) terrestrial gravity, (b) airborne gravity, (c) satellite-derived marine gravity, (d) GGM – XGM2019, (e) GDEM – SRTM and (f) distribution of GNSS Levelling Data

In the application of the KTH method for geoid modelling, the DEM plays a key role in topographic, atmospheric, and downward continuation corrections [26]. Shuttle Radar Topography Mission (SRTM) utilized in this study as the elevation information within a resolution of 1 arc second, extracted from the Open Topography website at https://portal.opentopography.org/raster?pentopo=OTSRTM.082015.4326.1 [27]. Geographical distribution of SRTM data can be seen in Figure 2(e).

2.2.6 GNSS levelling

An integral aspect of geoid computation involves evaluating the reliability of the computed geoids through a rigorous geoid validation process. The validation process aims to quantify the accuracy and consistency of the computed geoid heights by computing the RMSE between the geoid heights derived from the computed geoids and GNSS levelling data. To facilitate this validation process, a dataset comprising 45 GNSS levelling points (Figure 2(f)) has been obtained from DSMM. These GNSS levelling data were acquired using high-precision PPP methods via GIPSY-OASIS II and AUSPOS processing. The stations were not a random distribution but rather strategically chosen based on their association with tide gauges and existing MyRTKnet CORS infrastructure [28]. This comparative analysis serves as a measure to ascertain the reliability of the computed geoid models in interpolating geoid heights across the study area.

3. Methodology

3.1 First Strategy

The first strategy involves the commonly employed method to combine and grid airborne gravity anomalies data in the computation of gravimetric geoid, as demonstrated by [14]. This method emphasizes to simultaneously downward continuation the airborne gravity data and merging it with terrestrial and marine data in a single procedure, as illustrated in Figure 3. Before investigating the accuracy of the geoid, the airborne data underwent a buffering process employing four distinct buffer distances: 0 km, 1 km, 5 km, and 10 km from the terrestrial gravity data, as depicted in Table 2 and Figure 4. Based on Figure 4, the terrestrial and airborne gravity data are represented by brown and blue colours, respectively. The rationale behind implementing these buffer distances is to meticulously investigate the influence of the interpolation bridging degrees of gravity data accuracy to the overall precision of the gravimetric geoids. Furthermore, prior studies by [9], has stated similar issues where errors from downward continuation can be controlled through space-domain regularization and frequency-domain filtering. Hence, the implementation of these buffer zones allows a controlled investigation into how varying degrees of spatial overlap influence the final geoid accuracy.

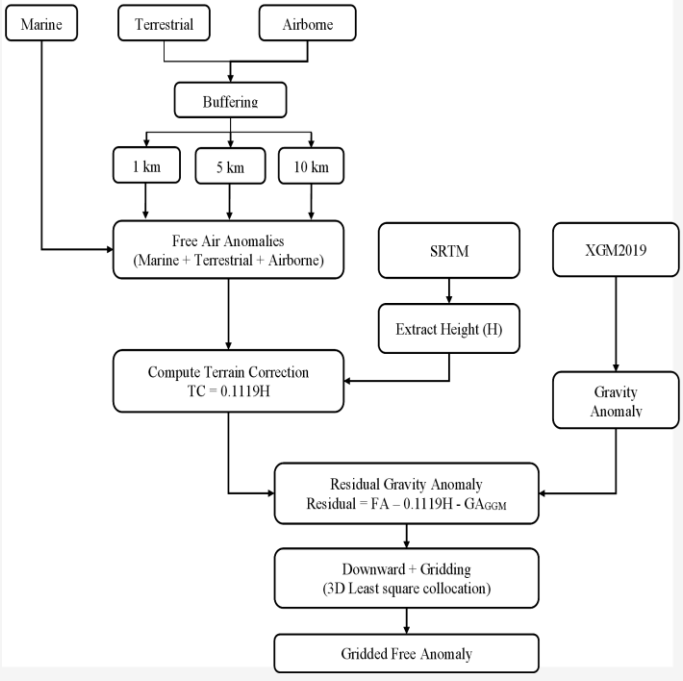

Figure 3: First strategy for geoid optimization

Table 2: Quantity of airborne gravity data after buffering

Buffer Distance	No. of airborne data
0 km	24855
1 km	22049
5 km	10124
10 km	6096

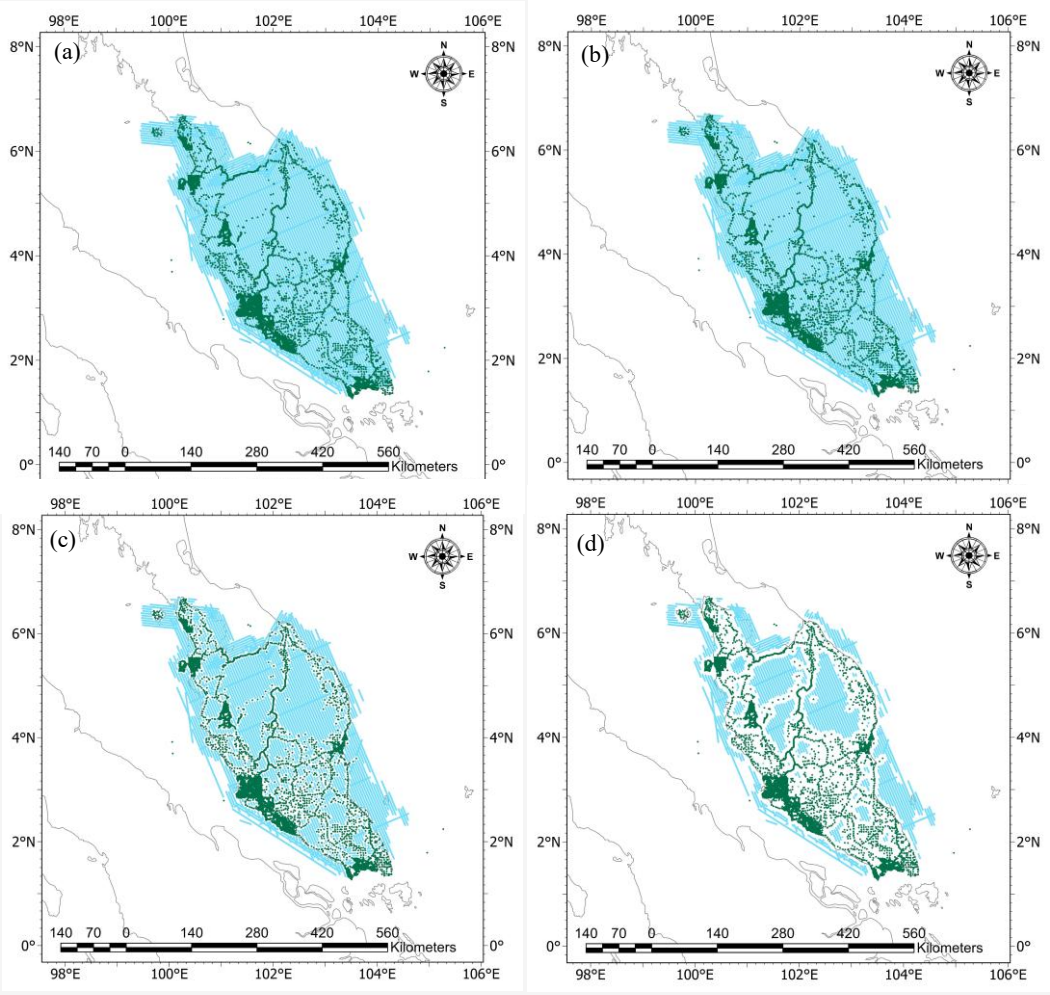

Figure 4: Terrestrial and buffered airborne gravity data of (a) 0 km, (b) 1 km, (c) 5 km and (d) 10 km

3.2 Second Strategy

The second strategy explores the effect on downward continuation of airborne gravity data while the process is executed separately. In this approach, airborne gravity anomalies are brought downward to the topographical surface before the combination and gridding. This strategy takes into consideration that airborne gravity anomalies are initially floating at a certain height as the data have been acquired at a certain flight height. It is proposed to test this approach against the first strategy, which is commonly used by geodesists in geoid determination, to assess whether it has a significant impact on the accuracy of gravimetric geoid models. Figure 5 depicts the methodology for the second strategy, and only 1 km buffered data are used as the sample to be tested against the first strategy. The selection of a 1 km buffer as the reference for this strategy was because second strategy was designed to assess an alternative downward continuation approach using this optimal buffer distance.

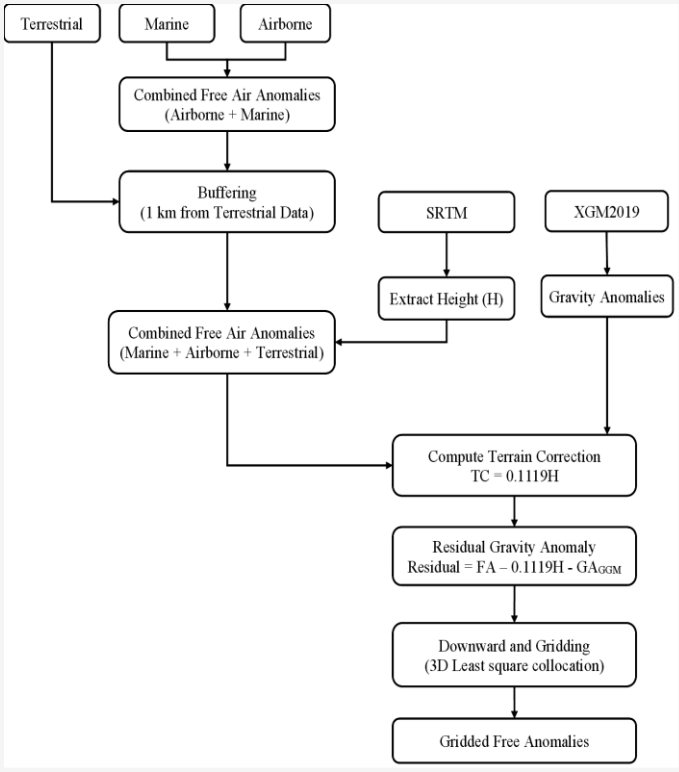

Figure 5: Second strategy for geoid optimization

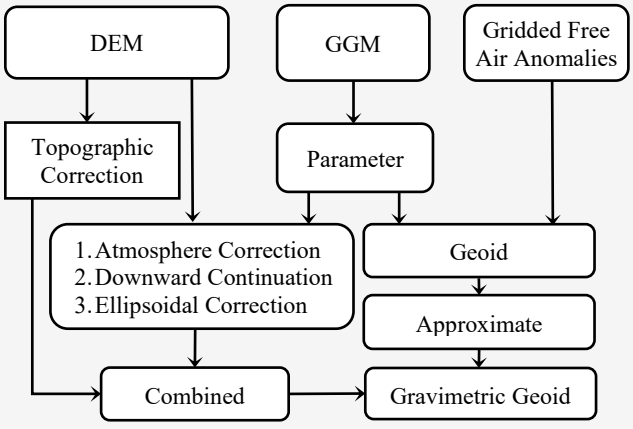

Figure 6: Overview of geoid modelling using LSMSA method

The analysis was deliberately limited to the 1 km buffer under the rationale that similar RMSE trends would likely persist across strategies, rendering further testing with broader, less accurate buffer distances unnecessary and methodologically redundant.

3.3 Geoid Computation using KTH Method

The computation of gravimetric geoids in this study implements the KTH method developed at the Royal Institute of Technology, Sweden (KTH) [29][30][31] and [32]. This method is favoured due to its convenience in computation to generate high-quality and precise geoid models [33] as it simplifies the combined topographic effect on geoid during computation [34]. The KTH method has been successfully implemented in geoid computation for several countries, including New Zealand, Sudan, Sweden, and Uganda. Figure 6 illustrates the overview of the KTH method (called "Least Square Modification of Stokes's Formula with Additive Correction (LSMSA)" as well).

3.3.1 Approximate Geoid

The approximate geoid is important in deriving geoid height based on GGM data, as stated in Equations 1 to 3 [30]. Prior to the approximate geoid computation in this study, XGM2019 has been integrated with gridded free air anomalies computed from the first and second strategies. The approximate geoid is added with the combined additive corrections for final gravimetric geoid computation.

$$\tilde{N} = \frac{R}{4\pi\gamma}\iint_{\sigma_0} S^L(\psi)\Delta g\,\sigma_0 + c\sum_{n=2}^{L} b_n \Delta g_n^{GGM}$$

Equation 1

$$S^L(\psi) = S(\psi) - \sum_{n=2}^{L}\frac{2n+1}{2} s_n P_n \cdot \cos(\psi)$$

Equation 2

$$b_n = \left(Q_n^L + S_n^*\right)\frac{C_n}{C_n + dC_n}$$

Equation 3

Where, $\tilde{N}$ is the approximate geoid height, R is the mean earth radius, γ is the mean normal gravity on the reference ellipsoid, $S^L(\Psi)$ is the modified Stokes' function to the modification limit, $S(\Psi)$ is the strokes original function, Ψ is the spherical distance from the computation point $(\emptyset, \lambda)$, s_nP_n is the legendre coefficients and polynomial of degree n, $cos\Psi = sin\emptyset \cdot sin\emptyset_i + cos\emptyset \cdot cos\emptyset_i cos(\lambda - \lambda_i)$, Δg is the terrestrial gravity anomaly, σ_0 is the spherical cap, $C = R/2\gamma$, L is the maximum degree of modification of Stokes' function, b_n is the vector of the least square parameter for the optimum solution where Q_n^L is residual spectrum component, s_n^* is the observed spectral coefficient, c_n is error variance, and dc_n is differential error from reference model. Δg_n^{GGM} is the Laplace harmonics of degree n calculated from the GGM [35].

a) Topographic Correction

In the KTH method, topographic correction is computed to add the topographic effect due to the undulation of terrains, particularly in Perak and Pahang states of Peninsular Malaysia. It is solved by a mathematical model in Equation 4, which is the combination of formula zero and first degree of direct and indirect topographic effects [36].

$$\delta N_{comb}^T(P) \approx -\frac{2\pi\mu}{\gamma}\left(H^2(P) + \frac{2H^3(P)}{R}\right)$$

Equation 4

Where $\delta N_{comb}^T(P)$ is the combined topographic correction, H is the topographic elevation and P is the computation point.

b) Downward Continuation

The Downward Continuation (DWC) correction is determined using the integration of SRTM and XGM2019 with M=360. Following [34], computation is performed using Equations 5 to 8.

$$\delta N_{dwc}^L = \delta N_{dwc}^{B,L} + \delta N_{dwc}^{te,L}$$

Equation 5

Where:

$$\delta N_{dwc}^{B,L} = \delta N_{dwc}^{B} + c\sum_{n=2}^{M}\left(s_n^* + Q_n^L\right)\Delta g_n$$

Equation 6

$$\delta N_{dwc}^{B} \approx \frac{H_P \Delta g_n^{GGM}}{\gamma} + 3\frac{H_P}{r_0}\zeta_P - \frac{H_P^2}{2\gamma_0}\left(\frac{\partial \Delta g}{\partial H_P}\right)$$

Equation 7

$$\delta N_{dwc}^{te,L} \approx \frac{R}{4\pi\gamma}\iint S^L(\psi)\left(H_P - H_0\right)\left(\frac{\partial \Delta_g}{\partial H_P}\right)_Q d\sigma_Q$$

Equation 8

From the equation, δN_{dwc}^L is the correction of downward continuation, $c = R/2\pi$, Q_n^L is the Molodensky truncation coefficient, s_n^* is the modification parameter, H_P and H_Q are the orthometric height of point P and Q that represent moving integration point, ζ_P is defined by Bruns' formula where T_P is the disturbing potential for point P and γ is the normal gravity at point P. Δg_n^{GGM} is Laplace harmonics computed from GGM. Δg is the surface of gravity anomaly, $d\sigma_0$ is the element of surface area at point Q on the reference sphere.

c) Atmospheric Correction

The atmosphere must be added or minimized in condition where masses outside the geoid are removed from gravity anomalies, in order to fulfil the Stokes' boundary condition [37]. The combined atmospheric correction is given in Equations 9 and 10:

$$\delta N_{comb}^{atm}(P) = \frac{\delta V_0^a}{\gamma} - \frac{2\pi R\rho_A}{\gamma}\left(\sum_{n=2}^{M}\left(\frac{2}{n-1} - s_n - Q_n^M\right)H_nP - \sum_{n=M+1}^{\infty}\left(\frac{2}{n+1} - \frac{n+1}{2n+1}Q_n^M\right)H_nP\right)$$

Equation 9

Where:

$$H_n(P) = \sum_{m=-n}^{n} H_{nm} \bar{Y}_{nm}(P)$$

Equation 10

From equation 9, δV_0^a is the term of zero degree at atmospheric potential, ρ_A is the atmospheric density at sea level which is approximately equal to 0.123 g /cm^3, Q_n^M is the spherical harmonic expansion coefficients of a reference atmospheric model. $H_n(P)$ is the Laplace surface harmonic of degree n for the topographic height. H_{nm} is amplitude of spherical harmonic coefficient and $\bar{Y}_{nm}$ is fully normalized spherical harmonic function that orthonormal over the sphere.

d) Ellipsoidal Correction

The modified version of Stokes' Formula that combine terrestrial gravity anomalies and GGM around computation point are commonly used to determine the final gravimetric geoid [17]. This is because, when GGM correctly applied at sea level, the remaining ellipsoidal correction for Stokes' formula is limited to the integration capsize. The correction for ellipsoidal is derived using Equation 11 as follows:

$$\delta N_e(P) = \frac{R}{2\gamma} \sum_{n=2}^{\infty} \left(\frac{2}{n-1} - s_n^* - Q_n^M \right) \left(\frac{a-R}{R} \Delta g_n^{GGM}(P) \right) + \frac{a}{R\left((\delta g_e)_n \right)}$$

Equation 11

Where $\delta N_e(P)$ is the equation of ellipsoidal correction, $s_n^* = s_n$ if $2 \le n \le M$ and $s_n^* = 0$, a is the semi-major axis, and, $(\delta g_e)_n$ is the Laplace harmonics of the ellipsoidal correction to the gravity anomaly. The final gravimetric geoids have been obtained by adding all the additive correction.

4. Result and Analysis

Four gravimetric geoid models have been computed using the first strategy and the data are as illustrated in Figure 7.

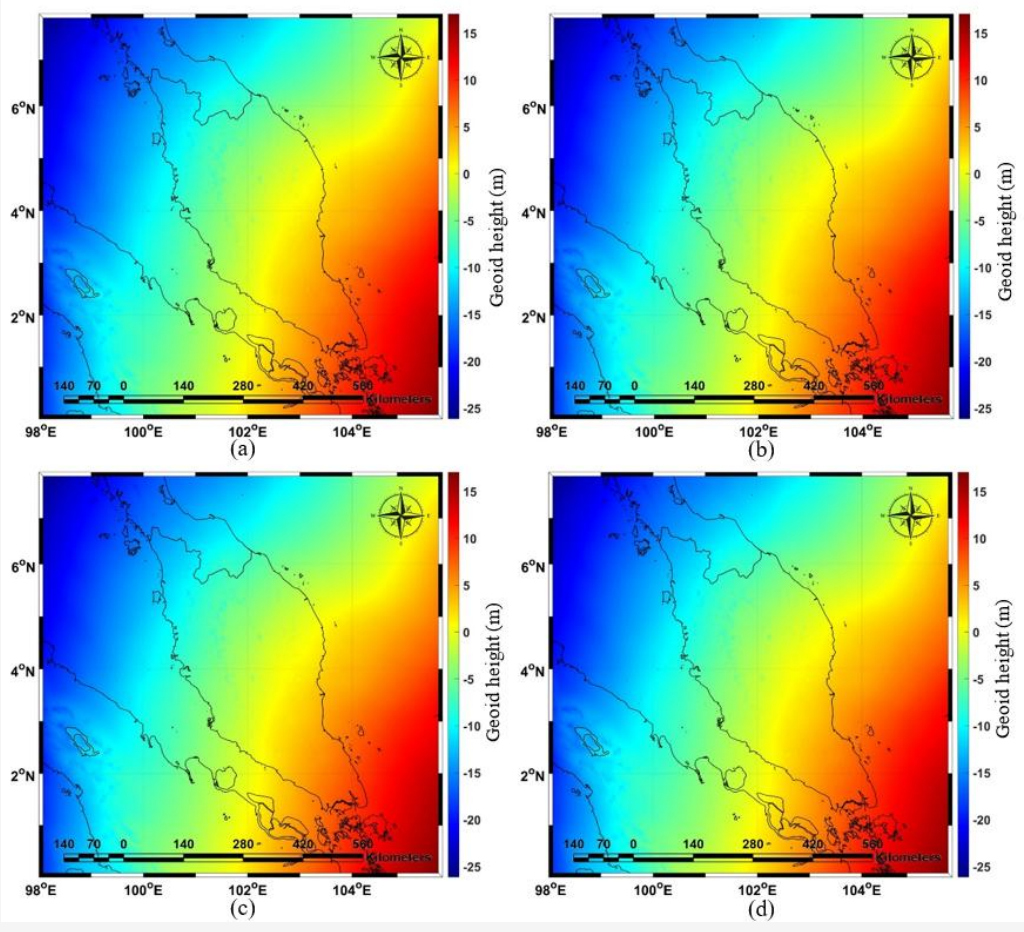

Figure 7: Computed gravimetric geoids using different buffer distances (a) 0 km, (b) 1 km, (c) 5 km, and (d) 10 km

The computed gravimetric geoid was validated against 45 GNSS levelling data to determine their external accuracies. Table 3 summarizes the statistical analysis of geoid validation using GNSS levelling data. The RMSE values for the models incorporating airborne data with buffer distances of 0 km, 1 km, 5 km, and 10 km are 0.047 m, 0.044 m, 0.048 m, and 0.057 m, respectively. These findings indicate that the geoid computed using a 1 km buffer distance yields the highest accuracy, with the smallest RMSE of 0.044 m indicating an improvement of 3 mm over the 0 km buffer (0.047 m). The residuals between geoid heights derived from GNSS levelling and those interpolated from the gravimetric geoid are illustrated in Figure 8. The graph reveals significant disparities where it is plausible that higher residual values may stem from inaccuracies in deriving geometrical geoid height from GNSS observations at the stations. The residual trends further show that geoid models using 0 km and 1 km buffers produce comparable results with minimal differences, whereas models using 5 km and 10 km buffers exhibit clear discrepancies, particularly at the first and ninth stations. These variations were likely influenced by the data thinning effect caused by the buffering process. As detailed in Table 2, the 5 km and 10 km buffer strategies result in the removal of a substantial portion of airborne data near terrestrial gravity points (as illustrated in Figure 4), thereby reducing data density. This reduction becomes more pronounced as the buffer distance increases which likely contributes to the diminished accuracy observed in the corresponding geoid models. An additional model was computed using the second strategy to be tested against the first strategy to combine and grid the gravity anomalies data. The gravimetric geoids produced from second strategy using 1 km buffered airborne data (Figure 9) and the statistical analysis for both strategies is tabulated in Table 4. Based on the table, the minimum, maximum, and mean values of the geoid height ranging from -16.166 m to -16.233 m, 8.773 m to 8.778 m, and -1.966 m to -1.971 m, respectively. Surprisingly, the RMSE value for both the first and second strategies exhibit an almost indistinguishable closeness, with a discrepancy of merely 0.001 m. This suggests that the proposed strategies exert negligible influence on the precision of the geoid model, indicating a lack of significant impact on its overall accuracy.

Table 3: Statistical analysis of geoids using first strategy

Buffer Distance	Min	Max	Mean	RMSE
0 km	-16.177	8.776	-1.968	0.047
1 km	**-16.233**	**8.773**	**-1.971**	**0.044**
5 km	-16.234	8.752	-1.983	0.048
10 km	-16.237	8.757	-1.977	0.057

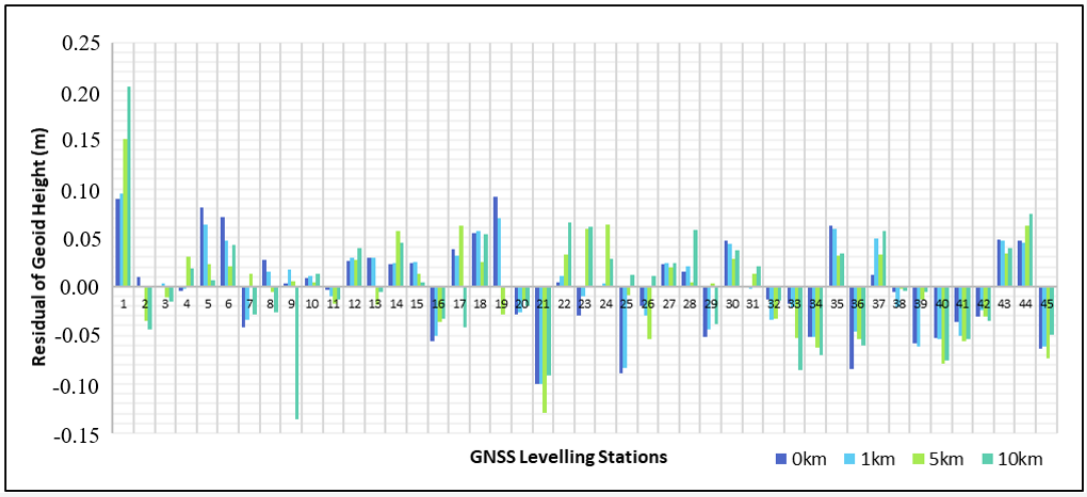

Figure 8: Residuals between GNSS levelling data with computed geoids using the first strategy

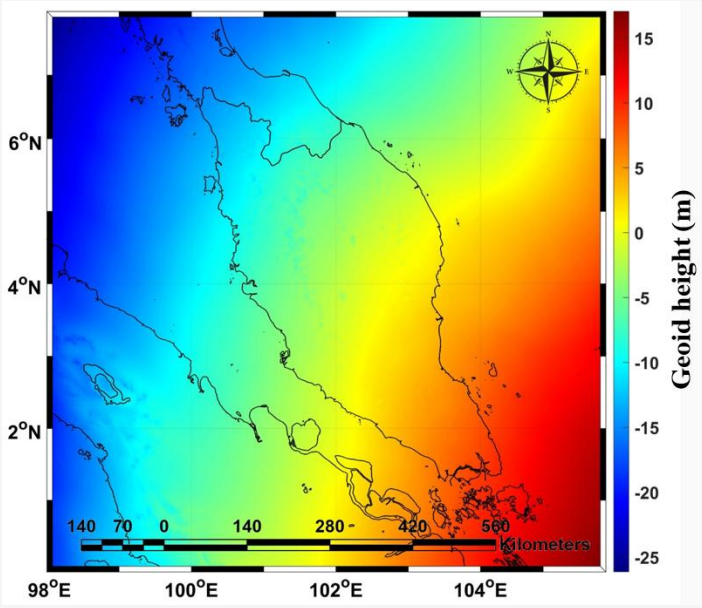

Figure 9: Gravimetric geoids derived using second strategy

Table 4: Statistical Analysis of gravimetric geoid models using the first and second strategy

Strategy	Min	Max	Mean	RMSE
First	-16.233	8.773	-1.971	0.044
Second	-16.166	8.778	-1.966	0.045

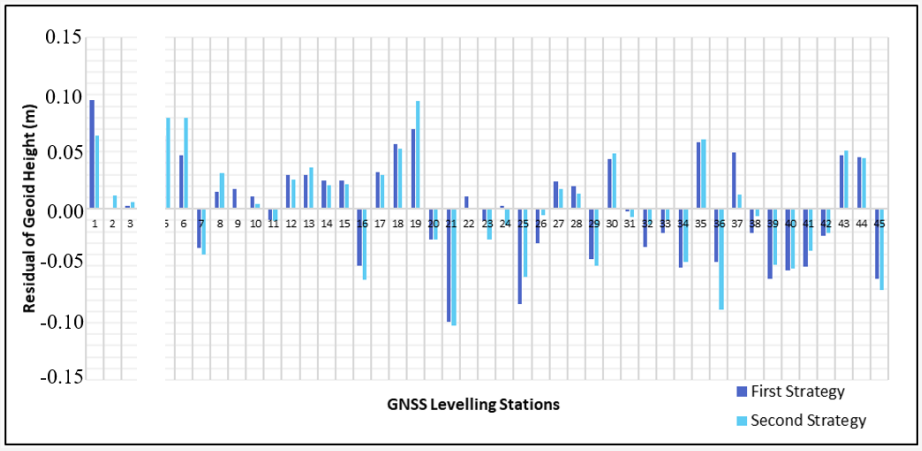

Figure 10: Residuals between 45 GNSS levelling data against gravimetric geoid models computed using first and second strategy

Table 5 presents the statistical results of the t-test conducted to assess potential bias between the two strategies. The analysis yields a t-value of 0.0029 and a p-value of 0.9977, which exceeds the 0.05 significance level for a 95% confidence interval. These results confirm that the mean residual differences between the two strategies are not statistically significant, suggesting that both approaches produce similar outcomes in the downward continuation process. A comparative residual between the first and second strategy using 45 GNSS levelling data are plotted and depicted in Figure 10. The graph indicates that while the RMSE from the validation results differs by only 1 mm, the interpolated geoid heights between the two strategies are not truly identical. The residuals, when tested against the 45 GNSS-levelling points are distributed within the range of 0.1 m to -0.1 m.

Table 5: T-Test analysis between two strategies (First and Second Strategy)

Strategy	N	Mean	STD	t-value	p-value
First	45	0.000002	0.044215	0.0029	0.9977
Second	45	-0.000004	0.045410		

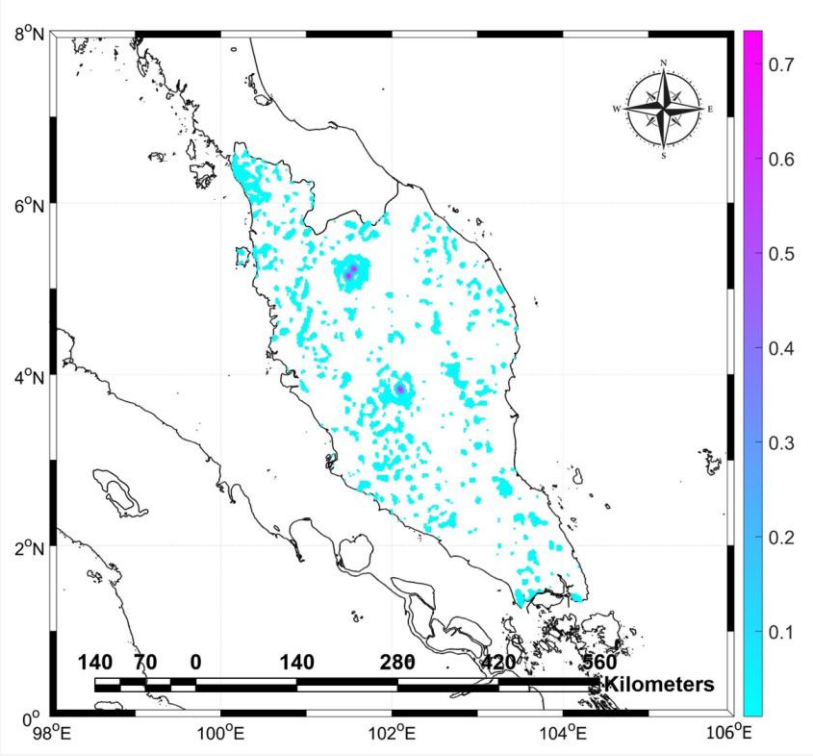

Figure 11: Comparative residuals of computed gravimetric geoids between first and second strategy

Furthermore, the residuals between the gravimetric geoid models from the first and second strategies in Figure 11, demonstrated that geoid height values from both models are distinct despite the near-identical accuracy. These discrepancies are most evident in the central region of Peninsular Malaysia, where the terrain elevation is high. This suggests that the downward continuation process produces varying effects depending on the strategy applied particularly in elevated areas. As highlighted in [38], higher flight altitudes in airborne gravity surveys tend to reduce the stability of downward continuation compared to lower-altitude measurements. Further investigation is recommended to identify the most optimal downward continuation approach for high-altitude airborne data.

5. Conclusion

In conclusion, two significant findings emerge from this research. The first finding reveals that the buffering process has a substantial impact on geoid model accuracy. The results demonstrate that a buffer distance of 1 km yields the highest accuracy, outperforming other buffer distances. These finding highlights that buffering airborne gravity data from terrestrial gravity data improves geoid model accuracy by 3 mm compared to computations without buffering. As the buffer distance increases, accuracy declines due to the decreasing density of airborne gravity data. With increasing buffer distances, more airborne data is excluded where the ratio of airborne data decreases significantly nearly halving with each increase from 1 km to 5 km to 10 km. Systematic analysis of these impacts provides empirical evidence of the nuanced relationship between buffering distance and geoid model accuracy. The second finding pertains to the combination and gridding of airborne gravity data in geoid modelling. Contrary to initial expectations, the results reveal a surprising convergence with minimal accuracy difference with mere 1 mm between two strategies. Additional statistical t-test analysis indicated t-value of 0.0029 and a p-value of 0.9977, which exceeds the 0.05 significance level for a 95% confidence interval.

This suggests the proposed second approach does not significantly manage to improve the geoid accuracy. Additionally, limitations arise from the spatial resolution of the grids and the assumptions applied during downward continuation, which can introduce inaccuracies especially in regions with complex topography. The study also assumes uniform data quality and stable flight conditions, which may not always be realistic in practical applications. Despite these challenges, the results provide useful recommendations for geoid development in similar environments. Nonetheless, these findings underscore the importance of investigating additional factors to achieve unprecedented levels of geoid precision. This research lays the groundwork for future studies aiming for 1 cm accuracy by elucidating the intricate relationship among buffering processes, data density, and data integration techniques, thereby offering valuable insights into geoid modelling optimization.

Acknowledgment
Special appreciation is extended to Universiti Teknologi MARA, Malaysia, for their generous financial support through the MyRA Research Grant (600-RMC5/3/GPM (069/2022)) and IPSIS Journal Support Fund. Sincere gratitude is also conveyed to the DSMM for providing the terrestrial and airborne gravity data, as well as the GNSS-levelling observations across Peninsular Malaysia.

References

[1] Yang, H. J., (2013). Geoid Determination Based on Combination of Terrestrial and Airborne Gravity Data in South Korea. *Journal of the Korean Society of Surveying Geodesy Photogrammetry and Cartography,* Vol. 31(6), 567-576. https://doi.org/10.7848/ksgpc.2013.31.6-2.567.

[2] Sulaiman, S. A., Talib, K., Mohd Yusof, O., Jaafar, J. and Md Wazir, M. A., (2014). Geoid Model Estimation without Addictive Correction using KTH Approach for Peninsular Malaysia. *FIG Congress 2014: Engaging the Challenges, Enhancing the Relevance*, Kuala Lumpur, June. 16-21, 2014, 1-14.

[3] Marotta, G. S. and Vidotti, R. M., (2017). Development of a Local Geoid Model at the Federal District, Brazil, Patch by the Remove-Compute-Restore Technique Following Helmert's Condensation Method. *Boletim de Ciencias Geodesicas*, Vol. 23(3), 520–538. https://doi.org/10.1590/S1982-21702017000300035.

[4] Jalal, S. J., Musa, T. A., Md Din, A. H., Wan Aris, W. A., Shen, W. B. and Pa'suya, M. F., (2019). Influencing Factors on the Accuracy of Local Geoid Model. *Geodesy and Geodynamics*, Vol. 10(6), 439–445. https://doi.org/10.1016/j.geog.2019.07.003.

[5] Jiang, T., (2018). On the Contribution of Airborne Gravity Data to Gravimetric Quasigeoid Modelling: A Case Study over Mu Us area, China. *Geophysical Journal International*, Vol. 215(2), 1308–1321. https://doi.org/10.1093/GJI/GGY346.

[6] Varga, M., Pitoňák, M., Novák, P. and Bašić, T., (2021). Contribution of GRAV-D Airborne Gravity to Improvement of Regional Gravimetric Geoid Modelling in Colorado, USA. *Journal of Geodesy*, Vol. 95(5). https://doi.org/10.1007/s00190-021-01494-9.

[7] Jabatan Ukur dan Pemetaan Malaysia. (2003). *Malaysia Geoid Model (MyGEOID)*. [Online] Available: https://www.jupem.gov.my/v1/wp-content/uploads/2016/04/Survey-General-Circular-Vol.-10-2005-on-MyGEOID.pdf. [Accessed: Dec. 15, 2024]

[8] Hwang, C., Hsiao, Y. S., Shih, H. C., Yang, M., Chen, K. H., Forsberg, R. and Olesen, A. V., (2007). Geodetic and Geophysical Results from a Taiwan Airborne Gravity Survey: Data Reduction and Accuracy Assessment. *Journal of Geophysical Research: Solid Earth*, Vol. 112(4). https://doi.org/10.1029/2005JB004220.

[9] Zhao, Q., Strykowski, G., Li, J., Pan, X. and Xu, X., (2017). Evaluation and Comparison of the Processing Methods of Airborne Gravimetry Concerning the Errors Effects on Downward Continuation Results: Case Studies in Louisiana (USA) and the Tibetan Plateau (China). *Sensors (Switzerland)*, Vol. 17(6). https://doi.org/10.3390/s17061205.

[10] Alberts, B. and Klees, R., (2004). A Comparison of Methods for the Inversion of Airborne Gravity Data. *Journal of Geodesy,* Vol. 78(1), 55–65. https://doi.org/10.1007/s00190-003-0366-x.

[11] Martinec, Z., (1996). Stability Investigations of a Discrete Downward Continuation Problem for Geoid Determination in the Canadian Rocky Mountains. *Journal of Geodesy*, Vol. 70, 805-828. https://doi.org/10.1007/BF00867158.

[12] Novák, P., Kern, M. and Schwarz, K. P., (2001). Numerical Studies on the Harmonic Downward Continuation of Band-Limited Airborne Gravity. *Studia Geophysica et Geodaetica*, Vol. 45(4), 327–345. https://doi.org/10.1023/A:1022028218964.

[13] McCubbine, J. C., Amos, M. J., Tontini, F. C., Smith, E., Winefied, R., Stagpoole, V. and Featherstone, W. E., (2018). The New Zealand Gravimetric Quasigeoid Model 2017 that Incorporates Nationwide Airborne Gravimetry. *Journal of Geodesy*, Vol. 92(8), 923–937. https://doi.org/10.1007/s00190-017-1103-1.

[14] Huang, J., Sideris, M., Vaníček, P. and Tziavos, I., (2003). Numerical Investigation of Downward Continuation Techniques for Gravity Anomalies. *Bollettino Di Geodesia e Scienze Affini*, Vol. 62.

[15] Li, X., Huang, J., Klees, R., Forsberg, R., Willberg, M., Slobbe, C., Hwang, C. and Pail, R., (2022). Characterization and Stabilization of the Downward Continuation Problem for Airborne Gravity Data. *Journal of Geodesy*, Vol. 96(18). https://doi.org/10.1007/s00190-022-01607-y.

[16] Sjöberg, L. E., Gidudu, A. and Ssengendo, R., (2015). The Uganda Gravimetric Geoid Model 2014 Computed by the KTH Method. *Journal of Geodetic Science*, Vol. 5(1), 35–46. https://doi.org/10.1515/jogs-2015-0007.

[17] Jiang, T., Dang, Y. and Zhang, C., (2020). Gravimetric Geoid Modeling from the Combination of Satellite Gravity Model, Terrestrial and Airborne Gravity Data: A Case Study in the Mountainous Area, Colorado. *Earth, Planets and Space*, Vol. 72(1), 1–15. https://doi.org/10.1186/s40623-020-01287-y.

[18] Muhammad Faiz, P., Ami Hassan, M. D., Ramazan, A. A., Noorfatekah, T., Mohamad Azril, C. A., Muhammad Zahir, R., Mohammad Hanif, H. and Nornajihah, M. Y., (2024). Integration of Local Mean Sea Level and Land Vertical Datum over Peninsular Malaysia Via Transformation Model. *Pure and Applied Geophysics*, Vol. 181, 3703-3721. https://doi.org/10.1007/s00024-024-03598-7.

[19] Jamil, H., Kadir, M., Forsberg, R., Olesen, A., Isa, M. N., Rasidi, S., Mohamed, A., Chihat, Z., Nielsen, E., Majid, F., Talib, K. and Aman, S., (2017). Airborne Geoid Mapping of Land and Sea Areas of East Malaysia. *Journal of Geodetic Science*, Vol. 7(1), 84-93. https://doi.org/10.1515/jogs-2017-0010.

[20] Sandwell, D., Müller, D., Smith, W., Garcia, E. and Francis, R., (2014). New Global Marine Gravity from CryoSat-2 and Jason-1 Reveals Buried Tectonic Structure. *Science*, Vol. 346(6205), 65–67. https://doi.org/10.1126/science.1258213.

[21] Vignudelli, S., Birol, F., Benveniste, J., Raynal, M. and Roinard, H., (2019). Satellite Altimetry Measurements of Sea Level in the Coastal Zone. *Surveys in Geophysics*, Vol. 40, 13-19. https://doi.org/10.1007/s10712-019-09569-1.

[22] Vignudelli, S., Kostianoy, A. G., Cipollini, P. and Benveniste, J., (2011). *Retracking Altimeter Waveforms Near the Coasts. Coastal Altimetry.* Springer Berlin Heidelberg. [Online]. https://doi.org/10.1007/978-3-642-12796-0.

[23] Cipollini, P., Calafat, F. M., Jevrejeva, S., Melet, A. and Prandi, P., (2017). Monitoring Sea Level in the Coastal Zone with Satellite Altimetry and Tide Gauges. *Surveys in Geophysics*, Vol. 38(1), 33–57. https://doi.org/10.1007/s10712-016-9392-0.

[24] Zingerle, P., Pail, R., Gruber, T. and Oikonomidou, X., (2020). The Combined Global Gravity Field Model XGM2019e. *Journal of Geodesy*, Vol. 94(7). https://doi.org/10.1007/s00190-020-01398-0.

[25] Muhammad Faiz, P., Ami Hassan, M. D., Abbak, R. A., Mohammad Hanif, H., Nornajihah Mohammad, Y., Muhammad Azril, C. A. and Mohd Adhar, A. S., (2022). Hybrid Geoid Model over Peninsular Malaysia (PMHG2020) using Two Approaches. *Studia Geophysica et Geodaetica*, Vol. 66(4), 98–123. https://doi.org/10.1007/s11200-021-0769-2.

[26] USGS EROS Archive - Digital Elevation Model - Shuttle Radar Mission Topography Mission (SRTM) 1 Arc-Second Global. *U.S Geological Survey.* [Online]. Available: https://www.usgs.gov/centers/eros/science/usgs-eros-archive-digital-elevation-shuttle-radar-topography-mission-srtm-1?qt-science_center_objects=0#qt-science_center_objects. [Accessed: Jan. 24, 2025].

[27] Cob, S., Kadir, M., Forsberg, R., Simons, W., Naeije, M., Din, A. H., Yacob, H., Amat, A., Mahdzur, D., Ibrahim, Z., Aziz, K., Yaacob, N., Johann, F., Jensen, T., Teitsson, H., Ses, S., Yahaya, A., Nordin, S., and Majid, F. (2022). Epoch-Based Height Reference System for Sea Level Rise Impact Assessment on the Coast of Peninsular Malaysia. *Remote Sensing*, Vol. 14(23). https://doi.org/10.3390/rs14236179.

[28] Sjöberg, L., (2003a). A Computational Scheme to Model The Geoid by The Modified Stokes Formula without Gravity Reductions. *Journal of Geodesy*, Vol. 77, 423–432. https://doi.org/10.1007/s00190-003-0338-1.

[29] Sjöberg, L., (2003b). A General Model for Modifying Stokes' Formula and its Least-Squares Solution. *Journal of Geodesy*, Vol. 77, 459–464. https://doi.org/10.1007/s00190-003-0346-1.

[30] Sjöberg, L., (2005). A Local Least-Squares Modification of Stokes' Formula. *Studia Geophysica et Geodaetica*, Vol. 49, 23–30. https://doi.org/10.1007/s11200-005-1623-7.

[31] Sjöberg, L. E. (2020). Unbiased Least-Squares Modification of Stokes' Formula. *Journal of Geodesy*, Vol. 94(9). https://doi.org/10.1007/s00190-020-01405-4.

[32] Ming, T. K., Zulkarnaini, M. A., and Ami Hassan, M. D. (2021). *Least Square Modification of Stokes Formulae with Additive Corrections Estimator for Klang Valley Geoid Modeling.* IOP Conference Series: Earth and Environmental Science, Vol. 620(1). https://doi.org/10.1088/1755-1315/620/1/012016.

[33] Ssengendo, R., (2015). A Height Datum for Uganda Based on A Gravimetric Quasigeoid Model and GNSS/levelling. *Architecture and the Built Environment, KTH Royal Institute of Technology*.

[34] Abdalla, A. and Fairhead, D., (2011). A New Gravimetric Geoid Model for Sudan using the KTH Method. *Journal of African Earth Sciences*, Vol. 60(4), 213-221. https://doi.org/10.1016/j.jafrearsci.2011.02.012.

[35] Abdalla, A. and Tenzer, R., (2011). The Evaluation of the New Zealand's Geoid Model using the KTH Method. *Geodesy and Cartography*, Vol. 37, 5–14. https://doi.org/10.3846/13921541.2011.558326.

[36] Danila, U., (2012). Mold2012: A New Gravimetric Quasigeoid Model over Moldova. *Architecture and the Built Environment, KTH Royal Institute of Technology.* https://www.diva-portal.org/smash/get/diva2:572006/FULLTEXT01.pdf.

[37] Tziavos, I. N., Andritsanos, V. D., Forsberg, R. and Olesen, A. V., (2005). Numerical Investigation of Downward Continuation Methods for Airborne Gravity Data. *International Association of Geodesy Symposia*, Vol. 129, 119–124. https://doi.org/10.1007/3-540-26932-0_21.